A Nonlinear Physics-Based Optimal Control Method for Magnetostrictive Actuators*

Ralph C. Smith
Department of Mathematics
Iowa State University
Ames, IA 50011
rsmith@iastate.edu

Abstract

This paper addresses the development of a nonlinear optimal control methodology for magnetostrictive actuators. At moderate to high drive levels, the output from these actuators is highly nonlinear and contains significant magnetic and magnetomechanical hysteresis. These dynamics must be accommodated by models and control laws to utilize the full capabilities of the actuators. A characterization based upon ferromagnetic mean field theory provides a model which accurately quantifies both transient and steady state actuator dynamics under a variety of operating conditions. The control method consists of a linear perturbation feedback law used in combination with an optimal open loop nonlinear control. The nonlinear control incorporates the hysteresis and nonlinearities inherent to the transducer and can be computed offline. The feedback control is constructed through linearization of the perturbed system about the optimal system and is efficient for online implementation. As demonstrated through numerical examples, the combined hybrid control is robust and can be readily implemented in linear PDE-based structural models.

*This research was supported in part by the Air Force Office of Scientific Research under the grant AFOSR F49620-95-1-0236.

1 Introduction

This paper addresses the development of a model-based nonlinear optimal control method for magnetostrictive actuators in structural applications. Such actuators utilize the 'giant' magnetostrictive effects provided by certain rare-earth compounds to produce significant strains in response to applied magnetic fields. As discussed in [7, 11], one core material which has proven very effective under a variety of operating conditions is Terfenol-D. Actuators utilizing this material can generate mechanical strains on the order of 500 $\mu strain$ in the linear range and up to 1000 $\mu strain$ in the nonlinear range. The materials are capable of generating forces in excess of 125 lbf with specific values highly dependent upon transducer design. Furthermore, the material provides a broadband response ranging from DC up to 20 KHz [17]. In combination, these qualities provide Terfenol-D transducers with significant capabilities as controllers and vibration absorbers in industrial and heavy structural applications. Such transducers have also been employed as sonar transducers and precision micropositioners.

The full utilization of magnetostrictive transducers in all such applications requires quantification of the transducer dynamics in response to various inputs. Magnetostrictive materials such as Terfenol exhibit inherent magnetic hysteresis which is significant at moderate to high drive levels. Furthermore, numerous investigations have demonstrated the stress and temperature sensitivity of the materials along with the nonlinear behavior of elastic properties such as the Young's modulus [8, 28, 37]. Finally, the magnetomechanical relation between input currents and output strains is nonlinear and displays significant hysteresis at high drive levels. All such hysteresis and nonlinear effects must be incorporated in both the transducer models and control laws to utilize the full capabilities of the actuators at high drive levels.

The magnetization model we employ is based upon an extension of the ferromagnetic mean field model of Jiles and Atherton [23, 24, 25, 33] while magnetostriction and hence strains are incorporated through a quadratic domain rotation model [23]. As demonstrated through validation experiments in [9], this combined model quantifies transducer dynamics for a large variety of prestresses and drive levels. The model also quantifies asymmetric minor loops which makes it appropriate for control design in structural applications which involve multiple frequencies and transient dynamics.

We concentrate here on linear structural models which incorporate this nonlinear actuator model. Such linear models are common in applications characterized by large forces but small displacements and provide a natural regime for initial development of a nonlinear control method which incorporates the actuator hysteresis and nonlinearities. A nonlinear open loop control is constructed first through the application of finite dimensional optimal control theory. This control adequately incorporates the hysteresis and nonlinearities inherent to the actuator but is not robust with regard to perturbations in operating conditions. Such robustness is provided by an additional feedback control constructed through linearization about the unperturbed optimal open loop control. The hybrid control containing the nonlinear open loop and linear perturbation closed loop components is highly robust, efficient to implement, and utilizes the flexibility and accuracy of the nonlinear actuator model to provide the capability for attenuating transient and broadband dynamics.

To place this control method in perspective, we briefly summarize existing control techniques for magnetostrictive actuators. For low drive level control applications, linear models and control methods have proven suitable for both bulk magnetostrictive actuators [5, 7, 31, 32]

and magnetostrictive particle actuators [29]. In a similar vein, the effects of hysteresis were also neglected and a linear law employed in [38] when designing a high precision magnetostrictive micropositioner. Such methods break down at moderate to high drive levels due to inherent hysteresis and nonlinearities [13]. For example, hysteresis provides a phase lag effect which will destabilize a system if unaccommodated. One technique for extending the linear range of transducer dynamics is based on the assumption that the underlying system is linear with nonlinear output harmonics acting as a disturbance. As demonstrated by Hall and Flatau [17] and Hodges and Sewell [19], feedback techniques can then be employed to reduce disturbances and improve linearity for certain operating regimes. Various nonlinear control techniques have also been employed for high drive level applications. Jenner et al [22] developed an active vibration controller for predescribed wave forms by considering a nonlinear control technique implemented through switching between positive and negative gains to the actuator. A similar objective was attained via neural network controllers by Bryant et al [4].

Control laws based upon Preisach models have also been employed for a variety of smart materials including magnetostrictives [14]. Such models are based upon polynomial or piecewise constant approximations to the nonlinearities and hysteresis loop, and are advantageous when the underlying physics is not well understood or quantified. Such characterizations provide a control input operator which is easily inverted (or has an inverse which is easily approximated) which facilitates control design based upon output linearization [36]. Feedforward control methods based upon Preisach models followed by linearization have been employed for piezoceramics [15] and are applicable for magnetostrictives in certain regimes.

The generality of Preisach models, which provides their advantage when the physics is not well understood, also leads to inherent limitations in many control applications. Because such models are not physics-based, they typically do not provide the capability for adapting to changes in operating conditions (e.g., drive levels, prestresses, minor loops) through the monitoring of system inputs. The transducer dynamics must be known a priori and incorporated directly in Preisach models whereas physics-based models of the type employed here can adapt to changing dynamic levels solely through the measurement or designation of input currents. This limits Preisach-based control laws to predefined trajectories (e.g., periodic) and does not provide the capability for directly attenuating unmodeled disturbances or inputs. Moreover, for unanticipated initial conditions, such methods also lack the capability for controlling transient dynamics. Finally, Preisach models typically require a large number of nonphysical parameters which limits their flexibility and increases implementation time in many applications.

The development of the physics-based control method is presented as follows. Section 2 contains a brief description of a typical magnetostrictive transducer along with an outline of the energy-based model employed in [9]. The modeling and approximation of transducer inputs to a thin beam are presented in Section 3. This provides the prototypical control system with nonlinear actuator inputs. The control problem is discussed in Section 4. Following an outline of nonlinear optimal control theory for finite dimensional systems, a linear optimal control method is considered. Numerical results demonstrate the success of the method at low drive levels and its failure at high drive levels due to unincorporated phase lag effects. An open loop nonlinear control method which fully incorporates material nonlinearities and hysteresis is then developed. Numerical examples are used to show that this method provides excellent attenuation when the system is known exactly but is not robust with respect to system

uncertainties. The final subsection of Section 4 illustrates the development and performance of a perturbation feedback control method obtained through linearization about the optimal control system. This feedback method provides excellent attenuation of structural dynamics, is highly robust with respect to operating uncertainties and is feasible for implementation. Finally, the method is effective for systems exhibiting broadband responses and both periodic and transient dynamics.

2 Magnetostrictive Actuator Model

The issues which must be addressed when developing a nonlinear modeling and control methodology are illustrated through consideration of the transducer depicted in Figure 1. This construction is typical for actuators currently employed in structural applications (see [16]), and its dynamics exhibit the full range of nonlinearities and hysteresis which must be characterized and incorporated in control design.

The primary components of the transducer consist of a magnetostrictive Terfenol-D rod, a surrounding wound wire solenoid, a surrounding permanent magnet, and a prestress mechanism consisting of spring washers and/or compression bolts. The input to the actuator consists of a time-dependent current $\mathcal{I}(t)$ to the solenoid. This generates a magnetic field H and corresponding magnetic flux B and magnetization M within the Terfenol rod. The rod is constructed so as to contain a large number of regions in which moments are aligned perpendicular to the longitudinal rod axis (the orientation of regions, termed domains, is further aligned by the prestress mechanism). The application of the magnetic field causes the rotation of these moments which in turn generates strains and forces within the material. This provides the mechanism for actuation. We note that the magnetostrictive materials can also be used for sensing through measurement of the magnetic fields generated by stress-induced domain rotations.

As illustrated in Figure 2, the relationship between the applied field H and the induced magnetization M displays significant hysteresis and saturation effects at high drive levels. This implies that the permeability μ, which relates the two, is a nonlinear, multivalued map. The magnetomechanical effects are also nonlinear as illustrated in Figure 3. At moderate drive levels, the relationship between the magnetization M and strain e is approximately quadratic,

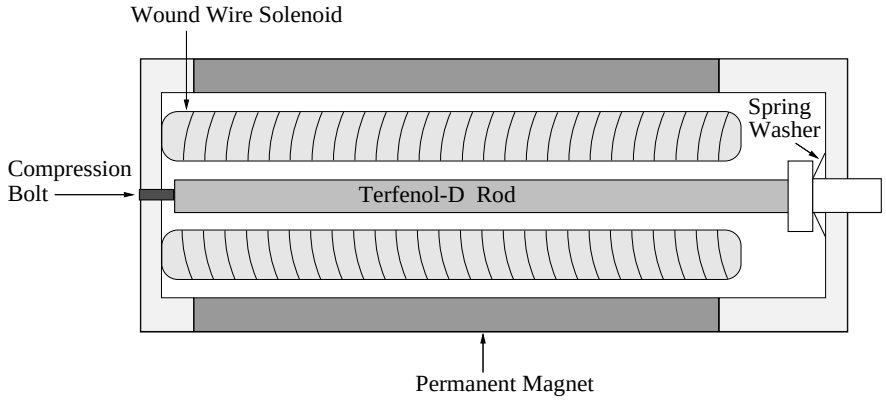

Figure 1. Cross section of a typical Terfenol-D magnetostrictive transducer.

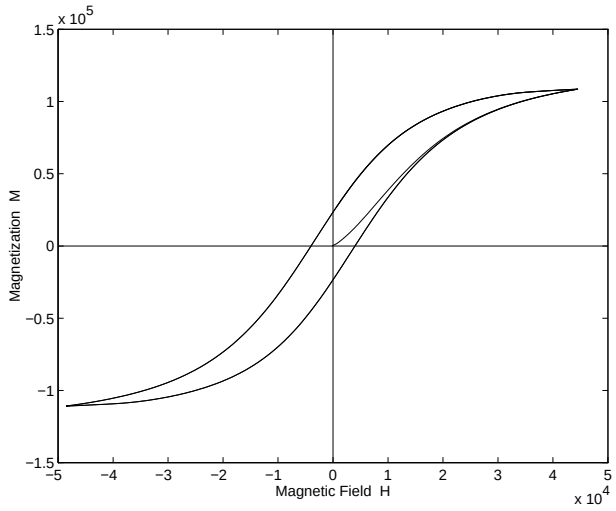

Figure 2. Relationship between the magnetic field strength H and the magnetization M.

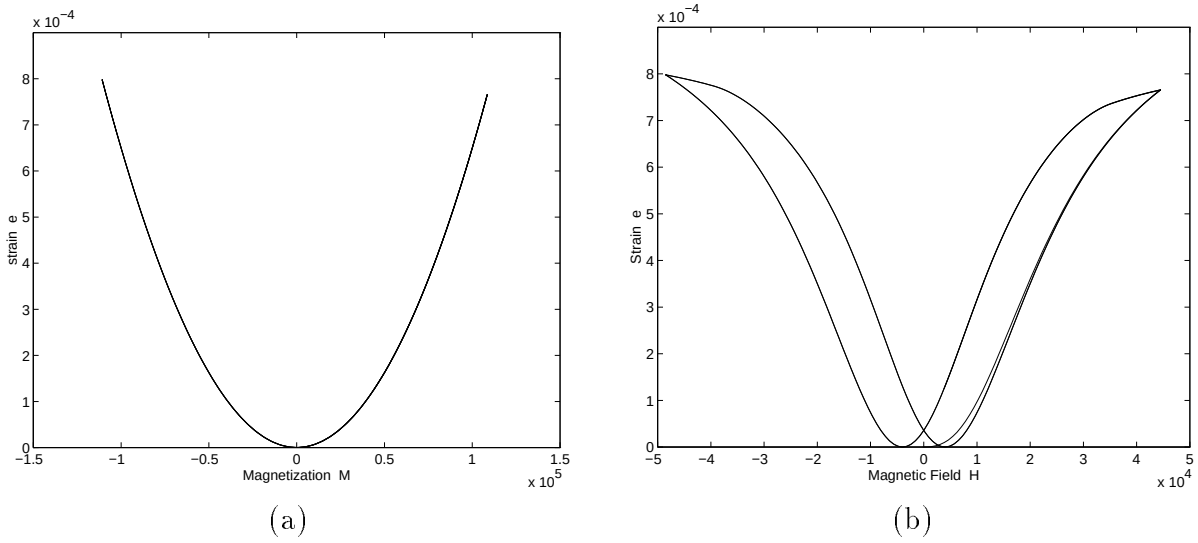

(a) (b)

Figure 3. (a) Input/output relationships; (a) magnetization M and strain e and (b) Magnetic field H and strain e.

as depicted in Figure 3a, which yields the 'butterfly' relationship shown in Figure 3b (the asymmetry is due to the use of experimental field input data when computing the modeled strain). As illustrated in [9], the magnetization/strain relation also exhibits hysteresis at high drive levels which must be incorporated in the magnetomechanical model.

The model described in [9] is used to characterize the transducer dynamics. The magnetization component of the model is based upon the Jiles-Atherton mean field theory for ferromagnetic materials [23, 24, 25, 33]. This theory is based on the quantification of energy losses due to domain wall intersections with inclusions or pinning sites within the material (the transition regions between domains are termed domain walls). For a material which is free from inclusions, the domain wall movement is reversible which leads to anhysteretic (hysteresis free) behavior. However, materials such as Terfenol contain second phase materials which

impede domain wall movement. At low field levels, domain wall movement about pinning sites is reversible and yields a reversible magnetization M_{rev}. At higher drive levels, domain walls intersect remote pinning sites which provides an irreversible component M_{irr}. It is this latter component which incorporates the energy loss and hysteresis in the model.

To characterize the total magnetization M, we consider first the effective field within the material. For rods subjected to a constant prestress σ_0, the effective field is given by

$$H_{eff}(t) = H(t) + \alpha M(t)$$

where

$$H(t) = n\mathcal{I}(t)$$

denotes the magnetic field generated by a solenoid having n turns per unit length with an input current $\mathcal{I}(t)$. The parameter α quantifies magnetic and stress interactions. Through thermodynamic considerations, the anhysteretic magnetization is then defined in terms of the Langevin function

$$M_{an}(t) = M_s \left[\coth\left(\frac{H_{eff}(t)}{a}\right) - \left(\frac{a}{H_{eff}(t)}\right) \right]. \tag{1}$$

Here M_s denotes the saturation magnetization of the material and a is a parameter which characterizes the shape of the anhysteretic curve. Energy balancing (see [24]) is then used to quantify the irreversible and reversible magnetizations through the expressions

$$\frac{dM_{irr}}{dt} = n\frac{d\mathcal{I}}{dt} \cdot \frac{M_{an}(t) - M_{irr}(t)}{k\delta - \alpha[M_{an}(t) - M_{irr}(t)]} \tag{2}$$

and

$$M_{rev}(t) = c[M_{an}(t) - M_{irr}(t)] \tag{3}$$

($\delta = \pm 1$ while the constants c and k are estimated from the experimental hysteresis curves). Finally, the total magnetization is given by

$$M(t) = M_{rev}(t) + M_{irr}(t)\,. \tag{4}$$

To first approximation, the strains generated by the material are given by the bulk magnetostriction

$$\lambda(t) = \frac{3}{2}\frac{\lambda_s}{M_s^2} M^2(t) \tag{5}$$

where λ_s denotes the saturation magnetostriction (see [23] for details). In combination, (1)-(5) characterize the relationship between the input current $\mathcal{I}$ and the strains generated by the transducer. Details regarding the well-posedness of the model are given in [35].

3 Structural Model

A structural system which has been experimentally employed to ascertain capabilities and properties of magnetostrictive transducers (see [10]) is illustrated in Figure 4. This system consisted of a cantilever beam with end-mounted actuators. Diametrically out-of-phase currents to the actuators generated bending moments which were used to attenuate transverse

beam vibrations. We will employ a model for this experimental setup as a prototype to illustrate the optimal control method proposed here.

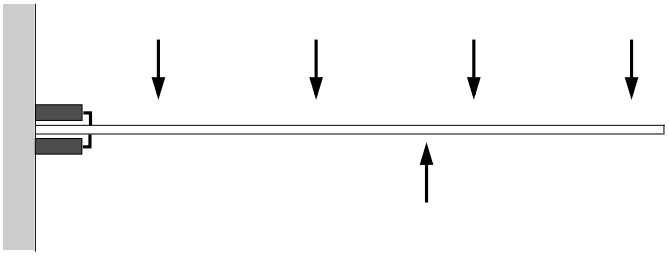

Figure 4. Cantilever beam with magnetostrictive actuators. Uniform force inputs are depicted above the beam while the measurement point is indicated by the lower arrow.

3.1 Thin Beam Model with Nonlinear Actuators

For modeling purposes, the beam is assumed to have length ℓ, width b, and thickness h. The density, Young's modulus, Kelvin-Voigt damping coefficient and air damping coefficient for the beam are denoted by ρ_b, E_b, c_{D_b} and γ, respectively. The cross-sectional area of the Terfenol rod is denoted by A_{mag} while the Young's modulus and damping coefficient for the Terfenol rod are denoted by E^H and c_D^H. The length and width of the connecting bar are denoted by ℓ_r and b_r, respectively, while the bar density is given by ρ_r. Finally, the transverse beam displacement is given by w while $g(t,x)$ denotes an exogenous surface force to the beam.

Moment and force balancing yields the strong form of the Euler-Bernoulli equations

$$\rho(x)\frac{\partial^2 w}{\partial t^2}(t,x) + \gamma\frac{\partial w}{\partial t}(t,x) + \frac{\partial^2 \mathcal{M}_{int}}{\partial x^2}(t,x) = g(t,x) + \frac{\partial^2 \mathcal{M}_{mag}}{\partial x^2}(t,x) \quad , \quad \begin{array}{l} 0 < x < \ell \\ t > 0 \end{array}$$

$$\left.\begin{array}{l} w(t,0) = \dfrac{\partial w}{\partial x}(t,0) = 0 \\ \mathcal{M}_{int}(t,\ell) = \dfrac{\partial \mathcal{M}_{int}}{\partial x}(t,\ell) = 0 \end{array}\right\} \quad , \quad t > 0 \ ,$$

along with appropriate initial conditions, as a model for characterizing the transverse beam dynamics. As detailed in [34], the composite density and internal bending moment are given by

$$\rho(x) = \rho_b hb + 2\rho_r b_r \ell_r \chi_{rod}(x)$$

$$\mathcal{M}_{int}(t,x) = EI(x)\frac{\partial^2 w}{\partial x^2}(t,x) + c_D I\frac{\partial^3 w}{\partial x^2 \partial t}(t,x)$$

where the characteristic function χ_{rod} delineates the location of the rods and

$$EI(x) = \frac{E_b h^3 b}{12} + 2A_{mag}E^H\left(h/2 + \ell_r\right)^2 \chi_{rod}(x)$$

$$c_D I(x) = \frac{c_{D_b} h^3 b}{12} + 2A_{mag}c_D^H\left(h/2 + \ell_r\right)^2 \chi_{rod}(x)\,.$$

For the case when the Terfenol rods are driven diametrically out-of-phase, the external moment is derived from (5) and is given by

$$\mathcal{M}_{mag}(t,x) = \mathcal{K}^M[M^2(t) + 2M(t)M_s]\chi_{rod}(x)$$

where $\mathcal{K}^M = (3\lambda_s/M_s^2)A_{mag}E^H(h/2+\ell_r)^2$. The inclusion of the weighted magnetization $2M(t)M_s$ provides the bias necessary to attain bidirectional strains.

To obtain a weak form of the model, we take the state to be the displacement w in the state space $X = L^2(0,\ell)$ with the inner product

$$\langle \phi, \psi \rangle_X = \int_0^\ell \rho\phi\psi \, dx \, .$$

The space of test functions is taken to be $V = H_L^2(0,\ell) \equiv \{\phi \in H^2(0,\ell) \,|\, \phi(0) = \phi'(0) = 0\}$ with the inner product

$$\langle \phi, \psi \rangle_V = \int_0^\ell EI\phi''\psi'' \, dx \, .$$

It should be noted that with these choices, V is continuously and densely embedded in H. Hence one has the Gelfand triple

$$V \hookrightarrow X \simeq X^* \hookrightarrow V^*$$

with the pivot space X.

A weak form of the model is then given by

$$\int_0^\ell \rho\ddot{w}\psi \, dx + \int_0^\ell \gamma\dot{w}\psi \, dx + \int_0^\ell \mathcal{M}_{int}\psi'' \, dx = \int_0^\ell \mathcal{M}_{mag}\psi'' \, dx + \int_0^\ell g\psi \, dx \tag{6}$$

for all $\psi \in V$. It is in this form that we develop the approximation method and formulate the control problem.

3.2 Approximation Method

A necessary step for constructing an implementable control law is the approximation of the infinite dimensional system (6). We employ a Galerkin approximation in the spatial variable to obtain a semidiscrete ODE system in time which is amenable to control formulation. Specifically, the spatial basis is taken to be $\{\phi_j\}_{j=1}^{m+1}$ where $\phi_j(x)$ denotes the j^{th} cubic B-spline modified to satisfy the fixed left boundary condition. Approximate solutions

$$w^m(t,x) = \sum_{j=1}^{m+1} w_j(t)\phi_j(x) \tag{7}$$

are then considered in the subpace $V^m = \text{span}\{\phi_j\}$. To obtain a vector ODE system, the infinite dimensional system (6) is restricted to V^m and posed in first-order form to yield

$$\begin{aligned} \dot{y}(t) &= Ay(t) + [B(u)](t) + G(t) \\ y(0) &= y_0 \, . \end{aligned} \tag{8}$$

The component system matrices have the form

$$A = \begin{bmatrix} 0 & I \\ \widetilde{Q}^{-1}K & \widetilde{Q}^{-1}C \end{bmatrix}$$

$$[B(u)](t) = \left[M^2(u) + 2M(u)M_s\right](t) \begin{bmatrix} 0 \\ \widetilde{Q}^{-1}\widetilde{B} \end{bmatrix}$$

$$G(t) = \begin{bmatrix} 0 \\ \widetilde{Q}^{-1}\tilde{g}(t) \end{bmatrix}$$

where $y(t) = [w_1(t), \cdots, w_{m+1}(t), \dot{w}_1(t), \cdots, \dot{w}_{m+1}(t)]$ and

$$[\widetilde{Q}]_{ij} = \int_0^\ell \rho\phi_i\phi_j\,dx \qquad [\widetilde{B}]_i = \mathcal{K}^M \int_{mag} \phi_i''\,dx$$

$$[K]_{ij} = \int_0^\ell EI\phi_i''\phi_j''\,dx \qquad [\tilde{g}(t)]_i = \int_0^\ell g(t,x)\phi_i\,dx \tag{9}$$

$$[C]_{ij} = \int_0^\ell c_D I\phi_i''\phi_j''\,dx\,.$$

Note that $u(t) = \mathcal{I}(t)$ denotes the control input to the system. For future development, it is useful to let $\vec{b}$ denote the $2(m+1)$ vector $\vec{b} = [0\,,\, \widetilde{Q}^{-1}\widetilde{B}]^T$ so that the control input can be written as

$$[B(u)](t) = \left[M^2(u) + 2M(u)M_s\right](t)\,\vec{b}\,. \tag{10}$$

The system (8) provides the constraints employed in the control problem.

3.3 System Parameters

For the examples which follow, the choice $m = 12$ was sufficient for resolving beam dynamics in the frequency range considered and all reported results were obtained with $m = 16$. The dimension of the state vector y was then 34×1 due to the inclusion of both displacement and velocity components.

The specific physical parameters employed in the examples are summarized in Table 1. It should be noted that the beam parameters are consistent with typical values for aluminum laboratory beams while the Terfenol parameters are within the range obtained for model fits to an experimental transducer [9]. For this choice of beam parameters, the first two natural frequencies for the system occur at 6.1 Hz and 38.3 Hz. To account for the effects of parameter discontinuities due the actuators and damping in the system, it was necessary to obtain these values through a fast Fourier transform (FFT) of time domain data resulting from a simulated impact to the beam (it is not possible to obtain analytic expressions through separation of variables). The driving frequency in the numerical examples will be chosen close to but not exactly concurrent with these natural frequencies.

Beam	Actuator	Terfenol
$E_b = 7.0861 \times 10^{10}\ N/m^2$	$E^H = 7.0 \times 10^{10}\ N/m^2$	$a = 7105\ A/m$
$\rho_b = 2863\ kg/m^3$	$\rho_r = 8524\ kg/m^3$	$k = 7002\ A/m$
$c_{D_b} = 9.3663 \times 10^5\ Ns/m^2$	$\ell_r = .0254\ m$	$\alpha = .007781$
$\gamma = .013\ Ns/m^2$	$b_r = .002\ m$	$c = 0.3931$
	$A_{mag} = .0064\ m^2$	$M_s = 1.3236 \times 10^5\ A/m$
		$\lambda_s = 9.96 \times 10^{-4}$

Table 1. Parameters for the beam and Terfenol transducer.

4 Control Problem

The general form of the finite dimensional control system under consideration is

$$\begin{aligned} \dot{y}(t) &= f(y(t), u(t), t) \\ y(t_0) &= y_0 \end{aligned} \tag{11}$$

with states $y(t) \in \mathbb{R}^{2(m+1)}$ and controls $u(t) \in \mathbb{R}^p$ where $p = 1$ for the case of a single actuator pair. As detailed in [6, 26, 27, 30], an appropriate performance index for minimization over the time interval $[t_0, t_f]$ is

$$J(u) = \psi(y(t_f), t_f) + \int_{t_0}^{t_f} L(y(t), u(t), t)\, dt \tag{12}$$

where the Lagrangian is given by

$$L(y(t), u(t), t) = \frac{1}{2}\left[y^T(t) Q y(t) + u^T(t) R u(t)\right] . \tag{13}$$

The nonnegative definite matrix Q and positive matrix R weight the state and control input while the function $\psi(y(t_f), t_f)$ penalizes large terminal values of the state. Energy considerations can be used to specify both Q and ψ. As detailed in [2], an appropriate choice of Q, which arises from the minimization of the kinetic and potential energies, is a multiple of the mass matrix. Similarly, the choice

$$\psi(y(t_f), t_f) = \frac{1}{2} y^T(t_f) \Pi_f y(t_f) \tag{14}$$

minimizes the final energy when Π_f is specified as a positive matrix. In the examples which follow, Q and Π_f were chosen as

$$Q = \begin{bmatrix} d_1 & \\ & d_2 \end{bmatrix} \begin{bmatrix} K & \\ & \widetilde{Q} \end{bmatrix} \quad , \quad \Pi_f = \begin{bmatrix} d_3 & \\ & d_4 \end{bmatrix} \begin{bmatrix} K & \\ & \widetilde{Q} \end{bmatrix} \tag{15}$$

where K and $\widetilde{Q}$ are given in (9) and $d_1, \cdots, d_4$ are integer weights.

The Hamiltonian associated with this system is

$$H(y, \lambda, u, t) = L(y, u, t) + \lambda^T f(y, u, t) \tag{16}$$

where $\lambda(t) \in \mathbb{R}^{2(m+1)}$ is the adjoint variable or Lagrange multiplier. It should be noted that the state equation (11) satisfies

$$\dot{y} = \frac{\partial H}{\partial \lambda}$$

where $\frac{\partial H}{\partial \lambda}$ denotes the gradient of H with respect to λ.

The minimization of (12) is constrained by the system (11). To pose this as an unconstrained optimization problem, we incorporate the constraints via the Lagrange multiplier and consider the modified performance index

$$\begin{aligned} \overline{J}(u) &= \frac{1}{2} y^T(t_f) \Pi_f y(t_f) + \int_{t_0}^{t_f} \left[L(y, u, t) + \lambda^T(t)[f(y, u, t) - \dot{y}] \right] dt \\ &= \frac{1}{2} y^T(t_f) \Pi_f y(t_f) + \int_{t_0}^{t_f} \left[H(y, u, t) - \lambda^T(t) \dot{y} \right] dt \,. \end{aligned} \tag{17}$$

The minimum of the constrained functional J occurs at the minimum of the unconstrained functional $\overline{J}$ which in turn occurs when $d\overline{J} = 0$ (see [6, 26, 27]). Enforcement of this condition yields the necessary adjoint condition

$$\begin{aligned} \dot{\lambda} &= -\frac{\partial H}{\partial y} \\ \lambda(t_f) &= \Pi_f y(t_f) \end{aligned} \tag{18}$$

and the stationary condition

$$\frac{\partial H}{\partial u} = 0 \,. \tag{19}$$

Note that the terminal condition on the adjoint variable is chosen to satisfy the transversality constraint for the system. This provides the framework employed in the finite dimensional linear, nonlinear and perturbation control methods discussed next.

State Tracking Problem

The goal in many applications entails the control of system dynamics to a specific trajectory $s(t)$ given observations

$$y_{ob}(t) = Cy(t), \tag{20}$$

in $\mathbb{R}^\ell$, of the state dynamics. An appropriate performance index for this case is

$$J(u) = \psi(Cy(t_f) - s(t_f), t_f) + \int_{t_0}^{t_f} L(y(t) - s(t), u(t), t)\, dt$$

where L and ψ are given by (13) and (14), respectively. The final time boundary condition for this choice is then

$$\lambda(t_f) = C^T \Pi_f \left[Cy(t_f) - s(t_f) \right] \,.$$

4.1 Linear Optimal Control

At low drive levels with magnetic biases, experimental data has indicated a nearly linear relation between input currents to the solenoid and strains output by the transducer. This is reflected in the model response and can be employed when designing a control method for such regimes. For low drive level applications, reasonable approximate models and control methods can be attained through linearization about an appropriate input u_0. One choice is the coercivity value $u_0 = u_c$ at which $M(u_c) = 0$. In this case, the approximate linear control operator B is

$$Bu(t) = 2M_s \frac{\partial M}{\partial u}(u_c)u(t)\,\vec{b}$$

where

$$\frac{\partial M}{\partial u} = n(1-c)\frac{M_{an} - M_{irr}}{k\delta - \alpha[M_{an} - M_{irr}]} + ncM_s\left[\frac{1}{a}\mathrm{csch}^2\left(\frac{H_{eff}}{a}\right) + \frac{a}{H_{eff}^2}\right].$$

Under this approximation, the corresponding first-order system is

$$\begin{aligned} \dot{y}(t) &= Ay(t) + Bu(t) + G(t) \\ y(0) &= y_0\,. \end{aligned} \tag{21}$$

The stationary condition (19) then yields the optimal control

$$u^*(t) = -R^{-1}B^T\lambda(t)$$

while the state constraint (21) and adjoint condition (18) yields the optimality system

$$\begin{aligned} \begin{bmatrix} \dot{y}(t) \\ \lambda(t) \end{bmatrix} &= \begin{bmatrix} A & -BR^{-1}B^T \\ Q & -A^T \end{bmatrix}\begin{bmatrix} y(t) \\ \lambda(t) \end{bmatrix} + \begin{bmatrix} G(t) \\ 0 \end{bmatrix} \\ y(t_0) &= y_0 \\ \lambda(t_f) &= \Pi_f y(t_f)\,. \end{aligned} \tag{22}$$

The construction of the optimal control requires the solution of the two-point boundary value problem (22). Due to the linearity of the system, however, a fundamental solution matrix can be employed to formulate the optimal control as

$$u^*(t) = -R^{-1}B^T[\Pi(t)y(t) - r(t)] \tag{23}$$

where $\Pi(t)$ solves the differential Riccati equation

$$\begin{aligned} -\dot{\Pi} &= A^T\Pi + \Pi A - \Pi BR^{-1}B^T\Pi + Q \\ \Pi(t_f) &= \Pi_f\,. \end{aligned} \tag{24}$$

The perturbation variable $r(t) \in \mathbb{R}^{2(m+1)}$ is obtained through integration of the final time system

$$\begin{aligned} \dot{r}(t) &= -\left[A - BR^{-1}B^T\Pi\right]^T r(t) + \Pi G(t) \\ r(t_f) &= 0\,. \end{aligned}$$

In this manner, the solution of a system with split conditions at the initial and final times is replaced by solution of systems with only final time conditions.

Two special cases are sufficiently common in applications to warrant further discussion. The first concerns the infinite time problem while the second characterizes Riccati solutions and optimal controls when input forces are periodic. It is important to note that in these cases as well as the general finite time formulation, the control (23) acts in a feedback manner on current states of the system. This will not be the case with the nonlinear control method.

4.1.1 Infinite Time Problems

For the strongly dissipative systems under consideration, it is reasonable to assume that (A, B) is stabilizable and (A, C) is detectable (see (20) for discussion of the observation operator C). In this case, as $t \to \infty$, y and u approach 0 at a sufficient rate to guarantee the existence of the performance index

$$J(u) = \frac{1}{2} \int_{t_0}^{\infty} \left[y^T(t) Q y(t) + u^T(t) R u(t) \right] \, dt \, . \tag{25}$$

The Riccati matrix used to characterize the feedback control (23) is the solution to the steady state algebraic Riccati equation

$$A^T \Pi + \Pi A - \Pi B R^{-1} B^T \Pi + Q = 0 \tag{26}$$

and is now constant. Similarly, the decay of solutions implies that the perturbation component is given by $r(t) \equiv 0$. Hence implementation of the method requires only the offline solution of a Riccati solution followed by online feedback on observed states.

4.1.2 Periodic Problems

A second case which commonly arises in applications is that in which the exogenous force $G(t)$ models periodic or oscillatory inputs to the system. If τ denotes the fundamental period for all frequencies present, an appropriate performance index is

$$J(u) = \frac{1}{2} \int_{0}^{\tau} \left[y^T(t) Q y(t) + u^T(t) R u(t) \right] \, dt \, .$$

Under the hypotheses of stabilizability and detectability, it is shown in [3, 12] that the optimal control (23) can be formulated in terms of the solution to the algebraic Riccati equation (26) and the solution to the periodic perturbation system

$$\begin{aligned} \dot{r}(t) &= - \left[A - B R^{-1} B^T \Pi \right]^T r(t) + \Pi G(t) \\ r(0) &= r(\tau) \, . \end{aligned} \tag{27}$$

This yields a feedback algorithm which is efficient to implement in many applications.

4.1.3 Numerical Example – No Exogenous Force

To illustrate the performance and limitations of the linear control method, we consider the use of the linear control law in the nonlinear system

$$\begin{aligned} \dot{y}(t) &= Ay(t) + [B(u)](t) \\ y(t_0) &= y_0 \end{aligned} \tag{28}$$

for various magnitudes of the initial value y_0. To obtain these values, the uniform force $g(t,x) = g_0 \sin(10\pi t)$ was applied to the uncontrolled beam for $t_0 = 0.45$ seconds and then terminated. The initial value y_0 was taken to be the state at the time t_0 when control was initiated. Control inputs were computed through minimization of the infinite time performance index (25) with $R = 5 \times 10^2$ and $d_1 = d_2 = 5 \times 10^8$ in the definition (15) for Q.

The implementation of the method in this manner provides a numerical illustration of effects which may be observed when control currents computing using a linear model and control law are fed back into the true physical system having nonlinear actuators. While we are not providing here the full convergence analysis and model fits to a physical apparatus, numerous experiments have demonstrated the validity of the model [9] and the trends illustrated by these numerical results.

The uncontrolled and controlled beam displacements at the point $\bar{x} = 3\ell/5$ (see Figure 4) with $g_0 = 1$ are plotted in Figure 5b while the displacements generated with $g_0 = 100$ are plotted in Figure 5d. The relationship between the input magnetic field $H = n\mathcal{I} = nu$ and magnetization M for the two cases are given in Figures 5a and 5d. It is noted that at the low drive level, the relationship between H and M is approximately linear and the feedback of the linear control u into the nonlinear system (28) is very effective. At the higher drive levels, however, the relationship between H and M displays significant hysteresis which leads to energy loss and time delays in the input. In this case, the linear control law (23) does not provide the capacity for accurately quantifying and incorporating the hysteresis and subsequent delays which in turn produces the loss in control authority observed in Figure 5d. This illustrates that while the linear control method can be effective at low drive levels, it does not provide the accuracy necessary for moderate to high drive level applications. For such regimes, control methods which incorporate the actuator nonlinearities are required.

4.1.4 Numerical Example – Periodic Exogenous Force

A second regime common in structural applications is that in which exogenous disturbances are periodic (e.g., oscillating mechanical components). In this case, a semidiscretization in the spatial variable yields a system of the form (21) where $G(t)$ is periodic. To illustrate, the spatial uniform exogenous force $g(t,x) = g_0 \sin(10\pi t)$ was applied throughout the time interval $[0, 2.5]$. The uncontrolled trajectories at $\bar{x} = 3\ell/5$ with $g_0 = 1, 100$ are plotted in Figure 6b and Figure 6d, respectively. Both cases exhibit a beat phenomenon due to the close proximity of the 5 Hz driving frequency with the 6.1 Hz natural frequency for the beam (see Section 2.3).

Controlling current were computed via (23) with intermediate perturbation solutions obtained through integration of the system (27). Inputs for the low and high drive level cases are illustrated in Figures 6a and 6c. As in the previous example, the linear control method is

highly effective at low drive levels where the linear model is accurate. At the high drive level in which the actuators are advantageous, however, the input exhibits significant hysteresis which acts as a phase delay to the system. The result is a loss in control authority to the extent that controlled beam trajectories actually have larger magnitudes than the uncontrolled beam. This further motivates consideration of a nonlinear control method.

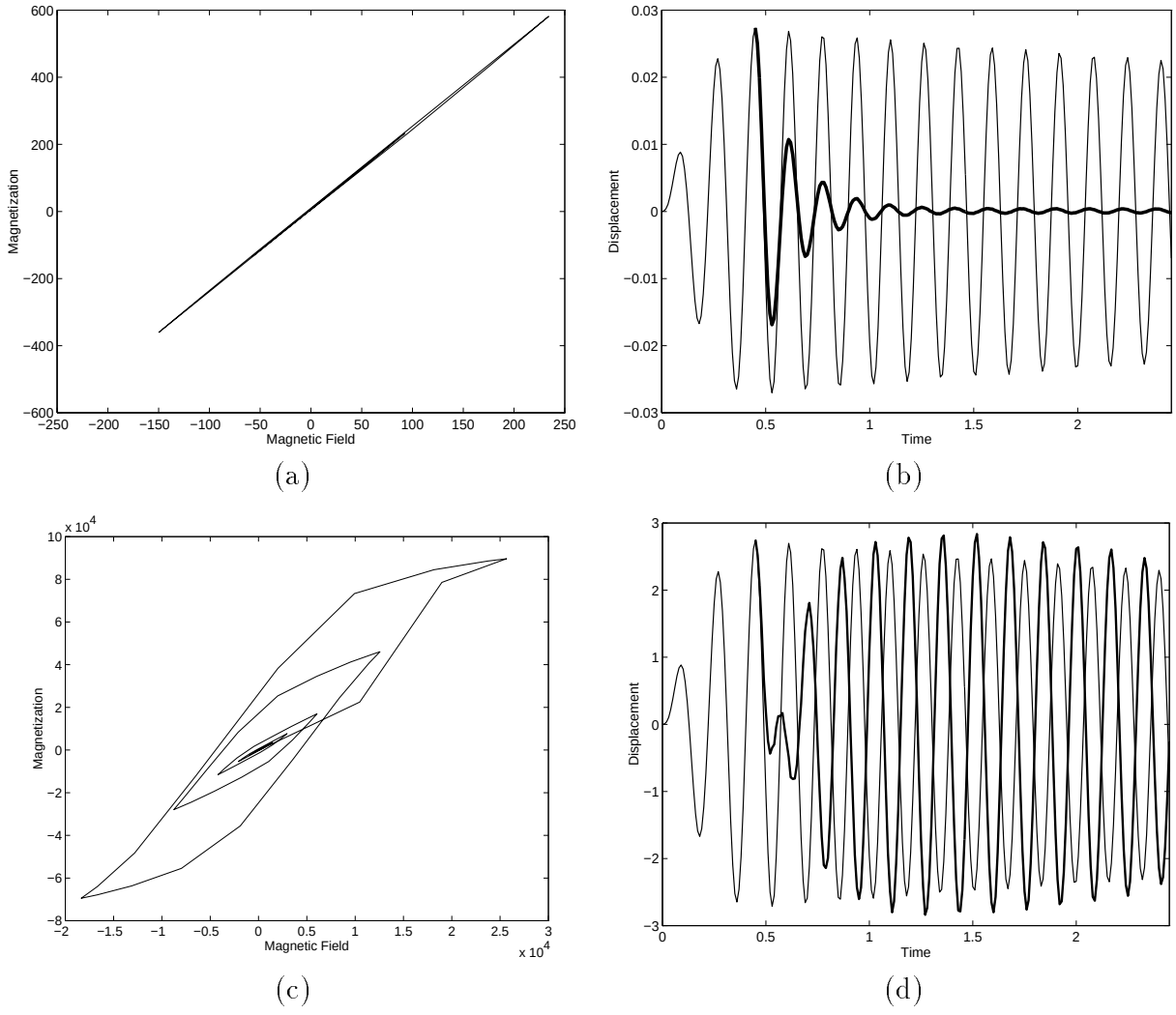

Figure 5. Feedback of linear law (23) into the nonlinear system (28). Relationship between magnetic field H and magnetization M; (a) $g_0 = 1$ and (c) $g_0 = 100$. Uncontrolled (——) and controlled (▬▬) beam trajectories at the point $\bar{x} = 3\ell/5$; (b) $g_0 = 1$ and (d) $g_0 = 100$.

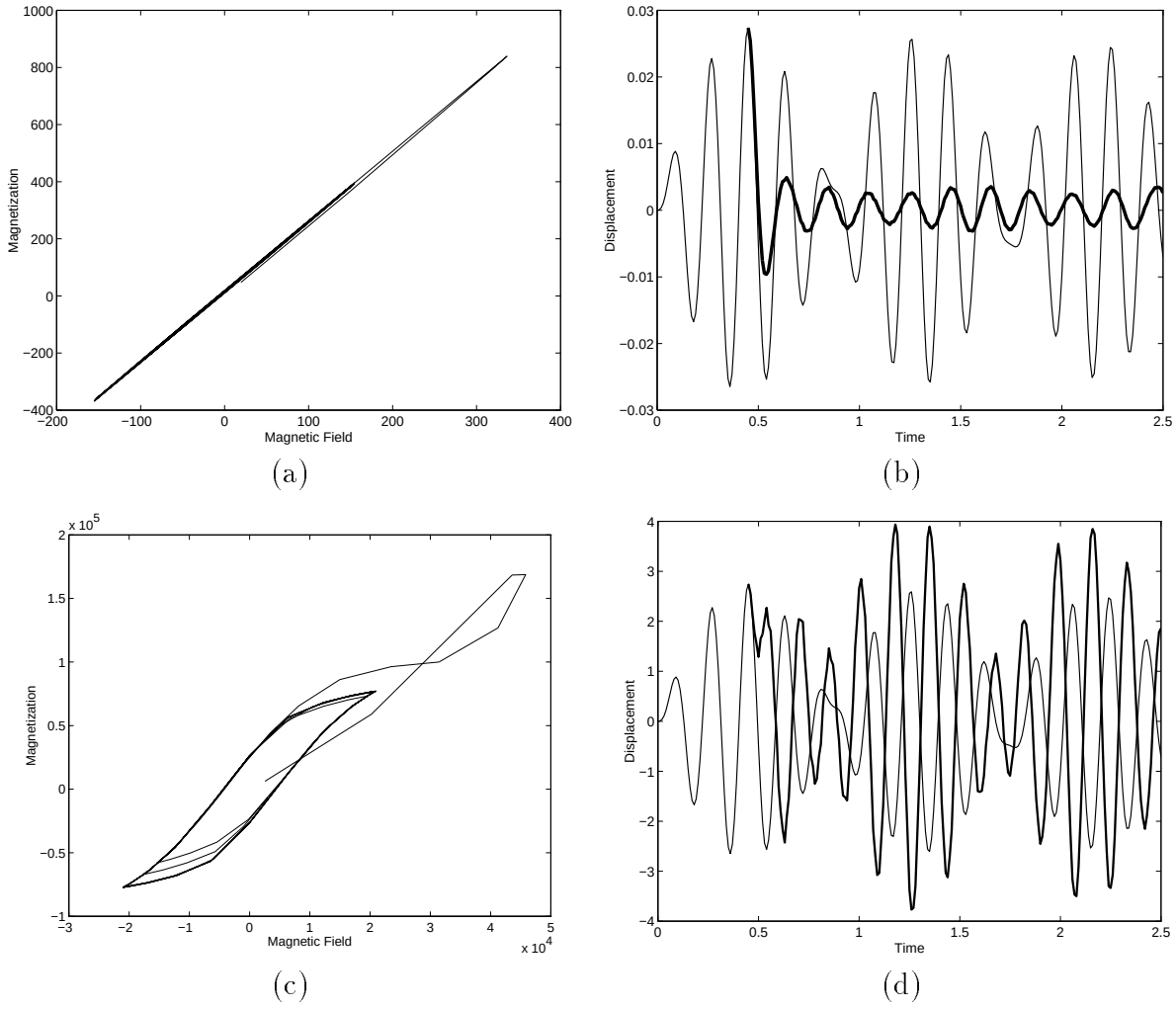

Figure 6. Feedback of linear law (23) into the nonlinear system (28). Relationship between magnetic field H and magnetization M; (a) $g_0 = 1$ and (c) $g_0 = 100$. Uncontrolled (——) and controlled (▬▬) beam trajectories at the point $\bar{x} = 3\ell/5$; (b) $g_0 = 1$ and (d) $g_0 = 100$.

4.2 Nonlinear Optimal Control

We consider here the problem of constructing a nonlinear control for the system

$$\begin{aligned} \dot{y}(t) &= Ay(t) + [B(u)](t) + G(t) \\ y(t_0) &= y_0 \,. \end{aligned} \tag{29}$$

In this case, minimization of the of the performance index (12) or (17) yields the optimality system

$$\begin{aligned} \begin{bmatrix} \dot{y}(t) \\ \dot{\lambda}(t) \end{bmatrix} &= \begin{bmatrix} Ay(t) + [B(u)](t) + G(t) \\ -A^T\lambda(t) + Qy(t) \end{bmatrix} \\ y(t_0) &= y_0 \\ \lambda(t_f) &= \Pi_f y(t_f) \end{aligned} \tag{30}$$

where the optimal control satisfies

$$u^*(t) = -R^{-1}[B_u^T(u^*)](t)\,\lambda(t).$$

Due to the nonlinear nature of the input operator $B(u)$, decomposition of the system matrices in terms of a fundamental matrix solution is not possible which prohibits efficient solution in terms of a Riccati matrix. To this end, we consider the approximation of the full two-point boundary value problem (30) or the equivalent first-order system

$$\begin{aligned} \dot{z}(t) &= F(t,z) \\ E_0 z(t_0) &= [y_0, 0]^T \\ E_f z(t_f) &= [0, \Pi_f y(t_f)]^T \end{aligned} \tag{31}$$

where $z = [y, \lambda]^T$ and

$$\begin{aligned} F(t,z) &= \begin{bmatrix} Ay(t) + [B(u)](t) + G(t) \\ -A^T\lambda(t) + Qy(t) \end{bmatrix} \\ E_0 &= \begin{bmatrix} I & 0 \\ 0 & 0 \end{bmatrix} \quad , \quad E_f = \begin{bmatrix} 0 & 0 \\ 0 & I \end{bmatrix}. \end{aligned} \tag{32}$$

Here I denotes a $2(m+1) \times 2(m+1)$ identity matrix where $m+1$ denotes the number of basis functions employed in the spatial approximation (7) of the state variables.

The solutions to the system (31) can be approximated through a variety of methods including finite differences and nonlinear multiple shooting. To illustrate a finite difference approach, we consider a discretization of the time interval $[t_0, t_f]$ with a uniform mesh having stepsize Δt and points $t_0, t_1, \cdots, t_N = t_f$. The approximate values of z at these times are denoted by $z_0, \cdots, z_N$. A central difference approximation of the temporal derivative then

yields the system

$$\begin{aligned} &\frac{1}{\Delta t}\left[z_{j+1}-z_j\right]=\frac{1}{2}\left[F(t_j,z_j)+F(t_{j+1},z_{j+1})\right] \\ &E_0 z_0=[y_0,0]^T \\ &E_f z_N=[0,\Pi_f y(t_f)]^T \end{aligned} \tag{33}$$

for $j=0,\cdots,N-1$.

The determination of a solution vector $z_h=[z_0,\cdots,z_N]$ to (33) can then be expressed as the problem of finding z_h which solves

$$\mathcal{F}(z_h)=0\,. \tag{34}$$

For the difference method and boundary conditions considered here, $\mathcal{F}(z_h)\in\mathbb{R}^{4(N+1)(m+1)}$ has the form

$$\mathcal{F}(z_h)=\begin{bmatrix} F_0 \\ F_1 \\ \vdots \\ F_j \\ \vdots \\ F_{N-1} \\ b(z_0,z_N) \end{bmatrix}, \qquad \begin{aligned} F_j &\equiv \frac{1}{\Delta t}\left[z_{j+1}-z_j\right]-\frac{1}{2}\left[F(t_j,z_j)+F(t_{j+1},z_{j+1})\right] \\ b(z_0,z_N) &= E_0 z_0+E_f z_N-\begin{bmatrix} y_0 \\ 0 \end{bmatrix}-\begin{bmatrix} 0 \\ \Pi_f y(t_f) \end{bmatrix}. \end{aligned}$$

A quasi-Newton iteration of the form $z_h^{k+1}=z_h^k+\xi_h^k$, where ξ_h^k solves

$$\mathcal{F}'(z_h^k)\xi_h^k=-\mathcal{F}(z_h^k), \tag{35}$$

is then used to approximate the solution to the nonlinear system (34). The $4(N+1)(m+1)\times 4(N+1)(m+1)$ Jacobian $\mathcal{F}'(z_h^k)$ has the form

$$\mathcal{F}'(z_h)=\begin{bmatrix} S_0 & R_0 & & & & \\ & S_1 & R_1 & & & \\ & & \ddots & \ddots & & \\ & & & & S_{N-1} & R_{N-1} \\ E_0 & & & & & E_f \end{bmatrix}$$

where

$$S_i=-\frac{1}{\Delta t}I-\frac{1}{2}\mathcal{A}(t_i)$$

$$R_i=\frac{1}{\Delta t}I-\frac{1}{2}\mathcal{A}(t_{i+1})\,.$$

The matrix $\mathcal{A}(t_i)$ is the linearization

$$\mathcal{A}(t_i)=\frac{\partial F}{\partial z}(t_i,z_i)$$

which yields the representation

$$S_i = -\frac{1}{\Delta t}\begin{bmatrix} I & 0 \\ 0 & I \end{bmatrix} - \frac{1}{2}\begin{bmatrix} A & \frac{\partial}{\partial \lambda}B[u_i^*] \\ Q & -A^T \end{bmatrix}$$

for S_i. The representation for R_i is similar.

For this application, direct solution of (35) is infeasible due to the large number of variables required to resolve the solution over a reasonable time interval. The structure of the Jacobian can be employed, however, to reduce both memory and computational requirements to the level of solving $4(m+1) \times 4(m+1)$ systems. To this end, we express the Jacobian in the analytic LU decomposition

$$\mathcal{F}'(z_h^k) = LU$$

where

$$L = \begin{bmatrix} S_0 & & & & \\ & S_1 & & & \\ & & \ddots & & \\ & & & S_{N-1} & 0 \\ E_0 & -E_0(S_0^{-1}R_0) & \cdots & E_0\prod_{i=1}^{N-2}(-1)^i(S_i^{-1}R_i) & E_f + E_0\prod_{i=1}^{N-1}(-1)^i(S_i^{-1}R_i) \end{bmatrix}$$

$$U = \begin{bmatrix} I & S_0^{-1}R_0 & & & \\ & I & S_1^{-1}R_1 & & \\ & & \ddots & \ddots & \\ & & & I & S_{N-1}^{-1}R_{N-1} \\ & & & & I \end{bmatrix}.$$

The solution of the system (35) is then obtained through direct solution of the system lower triangular system $L\zeta_h^k = -\mathcal{F}(z_h^k)$ followed by direct solution of the upper triangular system $U\xi_h^k = \zeta_h^k$.

Remark 1: The conditioning of the matrices S_i and R_i is partially governed by the choice of state weights d_1, d_2 in Q (see (15)). The conditioning is improved through the choice of values on the order of 10^3 or less. To maintain control authority, this dictates the choice of control weights R to be on the order of 10^{-3} or less. For these choices, the component matrices in the lower and upper diagonal systems are well conditioned.

Remark 2: The spatial approximation of the beam model was fully resolved with $m = 12$ basis functions and the results reported here were obtained with $m = 16$. This yields a total of $4(m+1)(N+1) = 13940$ coefficients to be obtained when using a stepsize of $\Delta t = .01$

on the time interval $[0.45, 2.5]$. To test the efficiency and memory requirements necessary for extending the method to problems in two space dimensions, we also ran the problem with $m = 144$ basis functions. This would correspond to a discretization with 12 basis functions in each spatial dimension and yields a total of 118,900 unknowns to be obtained. The method is sufficiently efficient so that even in this range, computations could be performed on a workstation in Matlab.

Remark 3: The matrix products arising in the lower triangular system L can be formed recursively. Moreover the component matrices have significant structure which can be utilized when forming the matrix products. The utilization of inherent recursions and structure is necessary when considering systems in two space dimensions which can have in excess of 500 states.

4.2.1 Numerical Example – No Exogenous Force

The use of the nonlinear control method is illustrated in the context of the cantilever beam driven for 0.45 seconds by the uniform force $g(t, x) = 100 \sin(10\pi t)$ at which point the force was terminated and control initiated. The control inputs were computed using the approximation method (33) for the two point boundary value problem (31) on the time interval $[t_0, t_f] = [0.45, 2.45]$. The control weights were taken to be $d_1 = d_3 = 5 \times 10^2$ and $R = 5 \times 10^{-4}$. This yielded an optimal current which was then applied as an open loop control to the system. The resulting controlled trajectory at the point $\bar{x} = 3\ell/5$ is compared with the uncontrolled trajectory in Figure 7. The corresponding relationship between the input magnetic field and output magnetization is plotted in Figure 8. It is noted that the model-based nonlinear control law very adequately incorporates the inherent hysteresis in the transducer and provides complete attenuation within 0.5 seconds of being invoked. This illustrates the performance of the nonlinear control law and capabilities of the magnetostrictive transducers under ideal operating conditions.

One difficulty with an open loop control law of this type is its lack of robustness with respect to uncertainties in operating conditions. Such uncertainties can be due to unmodeled dynamics, changing operating conditions, or slight delays or phase shifts due to filters, etc., and are present to some extent in all experimental systems.

To illustrate the effect of uncertainties on the performance of the open loop control, we consider the same system with the control applied 0.03 seconds late. This is a very reasonable scenario in experiments and must ultimately be accommodated by the control law. The uncontrolled and controlled trajectories for this case are depicted in Figure 9. The slight delay in the initiation of the control input results in a complete degradation of control authority (compare with the attenuation in Figure 7 with no delay). This illustrates the necessity of feeding back some form of state information and motivates consideration of perturbation control methods.

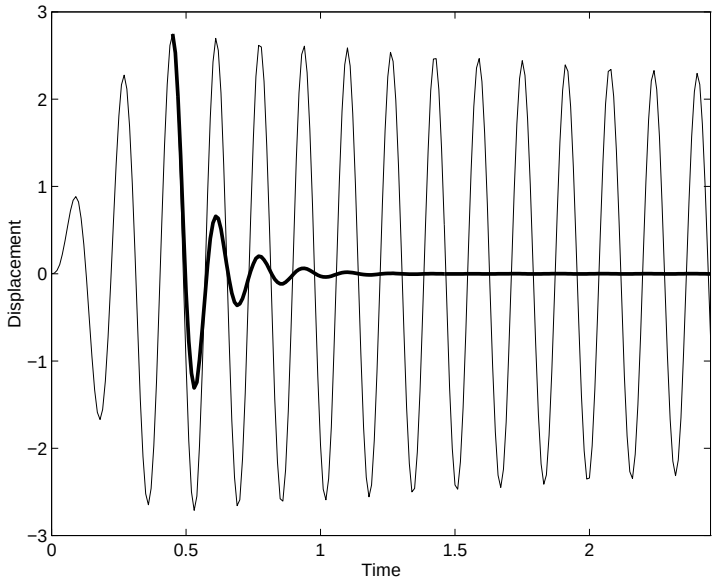

Figure 7. Uncontrolled and controlled beam trajectories at the point $\bar{x} = 3\ell/5$; —— (uncontrolled), ▬▬ (controlled).

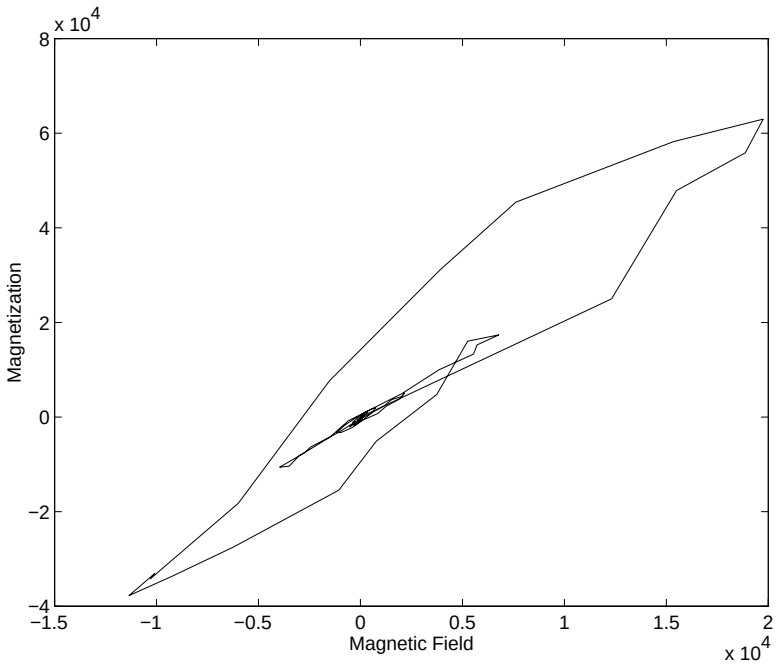

Figure 8. Input magnetic field $H = n\mathcal{I}$ and output magnetization M.

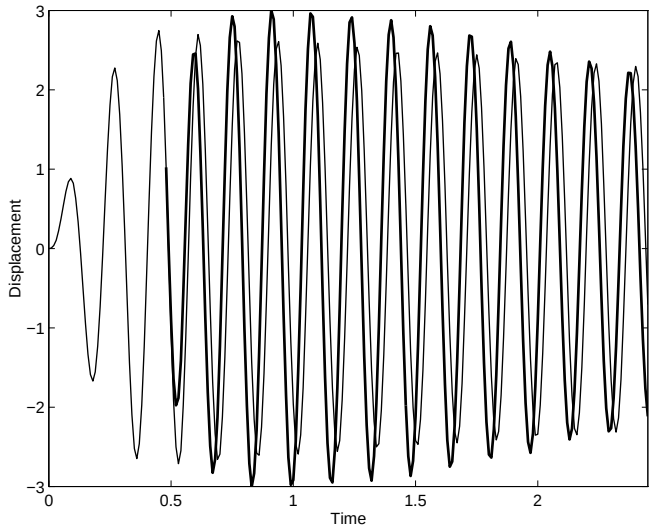

Figure 9. Uncontrolled and controlled beam trajectories at the point $\bar{x} = 3\ell/5$ with control initiated 0.03 seconds late; —— (uncontrolled), ▬▬ (controlled).

4.2.2 Numerical Example – Periodic Exogenous Force

The techniques for computing the open loop nonlinear control for systems with exogenous forces are identical to those employed in Section 4.2.1; one simply modifies F in (31) by the appropriate exogenous force. To illustrate, the force $g(t,x) = \sin(10\pi t)$ was applied for the full time interval [0.2.5] with the optimal control computed for the interval $[t_0, t_f = [0.45, 2.5]$. The resulting beam trajectory and inputs are plotted in Figure 10 and Figure 11. A comparison of Figures 10 and 6 indicates that reductions on the order of those obtained in the low drive level linear case can be obtained with the nonlinear law. Figure 11 illustrates that following an initial transient phase, the input relation settles into a hysteretic periodic cycle with the frequency matching that of the driving input.

In this case, the system is subject to uncertainties in the measured exogenous force in addition to the operating uncertainties discussed in Section 4.2.1. This can include perturbations in frequency or phase which can destabilize a feedback method and degrade open loop attenuation if unincorporated. In Figure 12, we illustrate the trajectories of a beam subjected to the force

$$g(t,x) = \begin{cases} 100\sin(10\pi t)\ , & t \leq .45 \\ 100\sin(14\pi t - 1.8\pi)\ , & .45 < t \leq 2.5 \end{cases}$$

with the factor of 1.8π included to ensure the continuity of g. The effect of the frequency change can be noted in that 12 oscillations are now present in the control interval $[.45, 2.5]$ compared with the 10 oscillations noted in Figure 10. The open loop control was computed for the assumed force $g(t,x) = 100\sin(10\pi t)$ and was applied 0.03 seconds late. It is noted that the control attenuation is completely degraded by these uncertainties and that further robustness must be incorporated in the method.

Remark 4: The persistence of beam vibrations in spite of the control input indicates a physical limitation of the actuator setup rather than a deficiency in the control formulation.

To attain greater attenuation, one must investigate controllability issues related to physical criteria such as actuator number and placement. The degree to which such physical issues play a role depends upon the application and in many cases, attenuation on the order of that observed in Figure 10 is sufficient.

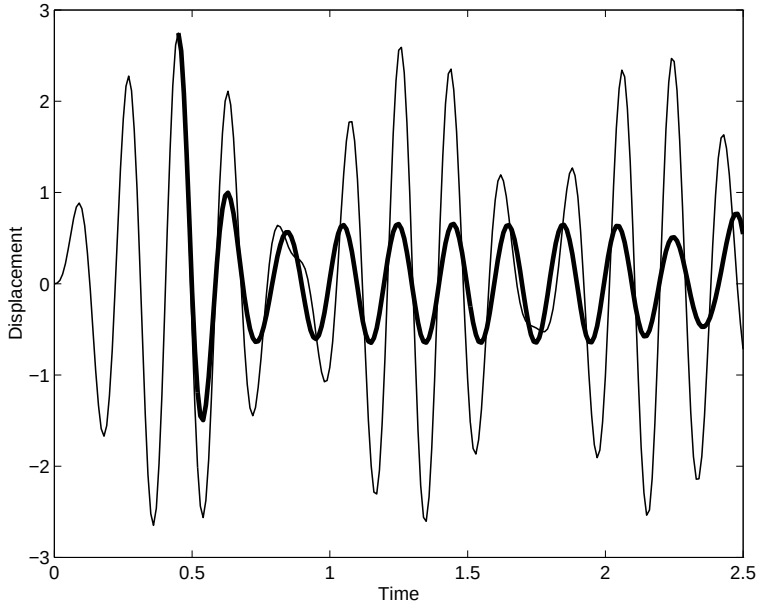

Figure 10. Uncontrolled and controlled beam trajectories at the point $\bar{x} = 3\ell/5$; —— (uncontrolled), ▬▬ (controlled).

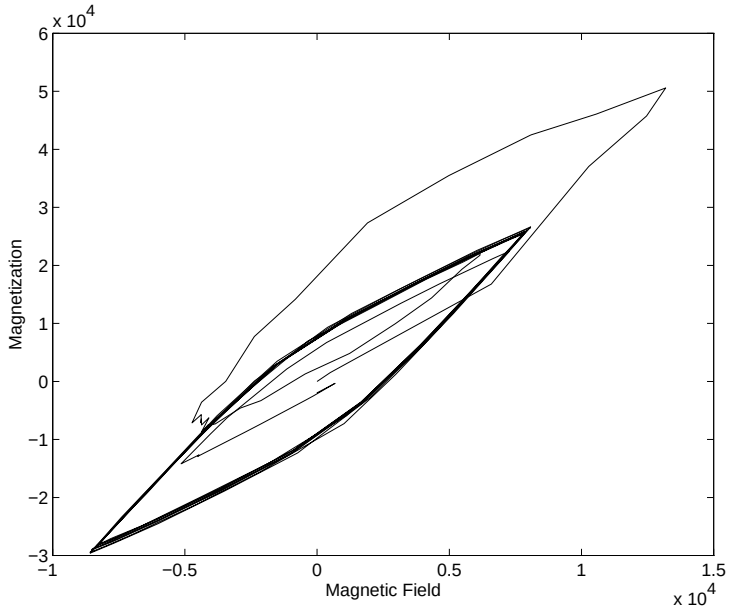

Figure 11. Input magnetic field $H = n\mathcal{I}$ and output magnetization M.

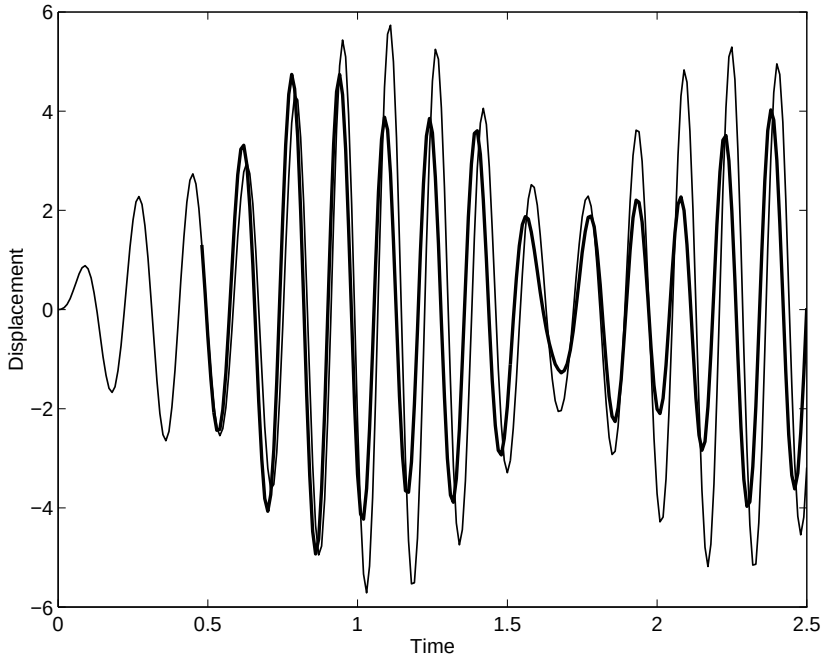

Figure 12. Uncontrolled and controlled beam trajectories at the point $\bar{x} = 3\ell/5$ with control initiated 0.03 seconds late and a 2 Hz frequency perturbation; —— (uncontrolled), ▬▬ (controlled).

4.3 Perturbation Control

As illustrated in the last example, a purely open loop control law suffers from lack of robustness with regard to system uncertainties. For various classes of uncertainties, robustness can be significantly enhanced through consideration of perturbation control techniques [6, 27]. In these methods, the system is linearized about the optimal control pair $(u^*(t), y^*(t))$ obtained through solution of the two-point boundary value problem (30) or (31). A feedback control $\delta u^*(t)$ is then designed to attenuate perturbations in the system due to uncertainties in the exogenous force or uncertainties in initial conditions as depicted in Figure 13. Both are common in applications with perturbed initial conditions often due to uncertainties in the starting time for the open loop control. Because LQR theory can be invoked to construct the perturbation control $\delta u^*(t)$, the implementation of the method is very efficient once the open loop control pair has been determined.

The perturbation control system can be obtained by expanding the augmented cost functional and constraint equations through higher-order terms and employing the simplifications provided by the fact that $u^*(t)$ and $y^*(t)$ minimize the first-order optimality system. Since $d\overline{J} = 0$ for the optimal pair $(u^*(t), y^*(t))$, expansion of the augmented cost criterion (17) through second-order terms and constraints to first-order yields

$$\delta^2 \overline{J} = \frac{1}{2} \int_{t_0}^{t_f} \left[\delta y^T \ \delta u^T \right] \begin{bmatrix} H_{yy} & H_{yu} \\ H_{uy} & H_{uu} \end{bmatrix} \begin{bmatrix} \delta y \\ \delta u \end{bmatrix} dt \tag{36}$$

and

$$\begin{aligned} \delta\dot{y}(t) &= A\delta y(t) + B\delta u(t) + \delta G(t) \\ \delta y(0) &= \hat{y}_0 \end{aligned} \tag{37}$$

where δu and δy are first-order variations about u^* and y^*. The optimal perturbation control δu^* is that which minimizes (36) subject to (37).

For the Hamiltonian (16), the second variation $\delta^2\overline{J}$ is given by

$$\delta^2\overline{J} = \frac{1}{2}\int_{t_0}^{t_f} \{\langle Q\delta y, \delta y\rangle + \langle R\delta u, \delta u\rangle\}\, dt \tag{38}$$

so that the LQR theory outlined in Section 4.1 can be directly employed to obtain $\delta u^*(t)$ and $\delta y^*(t)$. The overall control for the system is then taken to be $u^*(t) + \delta u^* t(t)$ with the optimal state given by $y^*(t) + \delta y^*(t)$. For implementation purposes, it should be noted that the optimal open loop control $u^*(t)$ can be computed offline leaving only $\delta u^*(t)$ to be computed online.

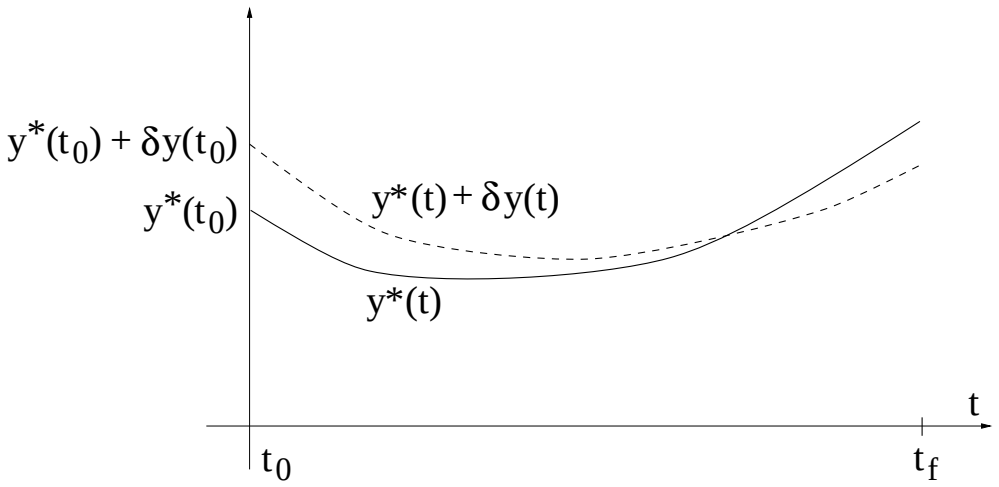

Figure 13. Optimal open loop controlled state and neighboring state due to perturbed initial condition.

4.3.1 Numerical Example – No Exogenous Force

The performance of the method is first illustrated in the context of Example 4.2.1 in which a perturbed initial value is introduced through application of the optimal control $u^*(t)$ to the system 0.03 seconds late. As noted in Figure 9, this perturbation is sufficient to destroy the authority of the open loop control.

To accommodate these perturbations, we employ the control law

$$\delta u^*(t) = -R^{-1}B^T\Pi\delta y(t)$$

where Π satisfies the algebraic Riccati equation (26). The resulting control trajectory is illustrated in Figure 14. It is noted that through the use of the feedback perturbation control, attenuation comparable to that for the unperturbed system (see Figure 7) is obtained. This provides a significant enhancement of the method with respect to perturbations in initial conditions.

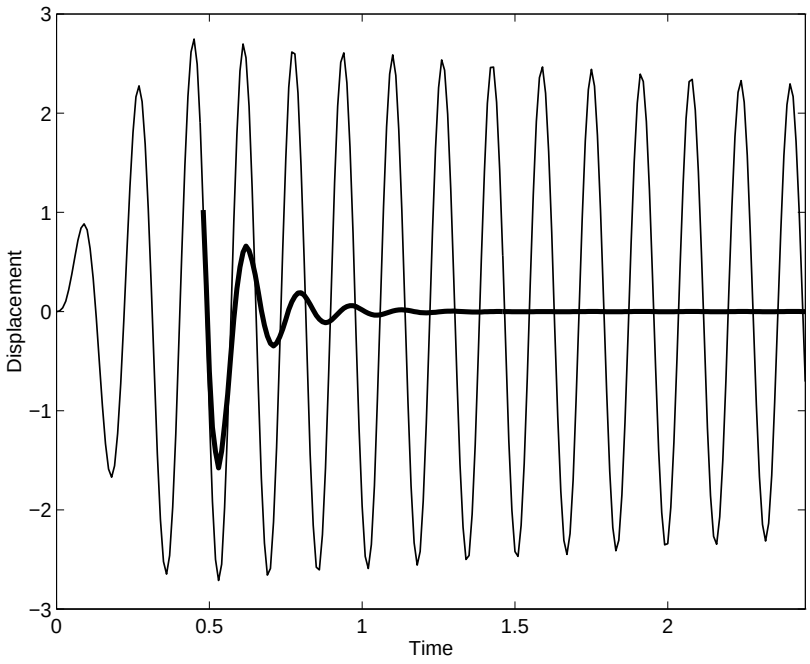

Figure 14. Uncontrolled and controlled beam trajectories at the point $\bar{x} = 3\ell/5$ with control initiated 0.03 seconds late; —— (uncontrolled), ▬▬ (controlled).

4.3.2 Numerical Example – Periodic Exogenous Force

Systems driven by an exogenous force are subject to force perturbations in addition to initial uncertainties or delays in control implementation. As illustrated in Example 4.2.2, perturbations from the expected 5 Hz force to a measured 7 Hz force completely degrade the open loop control. In this case,

$$\delta g(t,x) = 100[\sin(14\pi t - 1.8\pi) - \sin(10\pi t)]$$

over the time interval $[0.45, 2.5]$, and the perturbation control has the form

$$\delta u^*(t) = -R^{-1}B^T\left[\pi\delta y^*(t) - \delta r(t)\right]$$

where $\delta r(t)$ solves

$$\begin{aligned}\delta\dot{r}(t) &= -\left[A - BR^{-1}B^T\Pi\right]^T\delta r(t) + \Pi\delta G(t)\\ \delta r(0) &= \delta r(\tau)\,.\end{aligned}$$

In addition to the force perturbation, a perturbed initial condition due to a 0.03 second delay in control initiation was included in the system.

The uncontrolled and controlled beam trajectories at the point $\bar{x} = 3\ell/5$ are compared in Figure 15. It is noted that while the trajectories differ in frequency due to the combined open and closed loop effects, significant attenuation is attained throughout the time interval due to the feedback perturbation control component. A comparison with Figure 10 indicates that the controlled trajectory is comparable in magnitude to that in the perturbed case even

though the uncontrolled displacement is significantly larger. Such attenuation levels have also been noted with larger frequency perturbations (e.g., a perturbed driving frequency of 18 Hz). Hence the perturbation control provides a feedback methodology which is highly robust as well as efficient to implement.

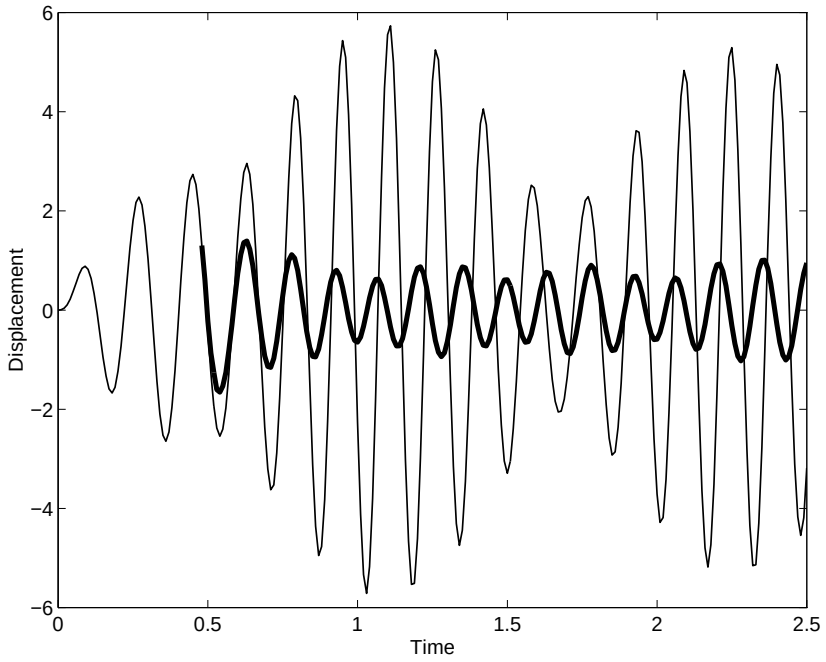

Figure 15. Uncontrolled and controlled beam trajectories at the point $\bar{x} = 3\ell/5$ with a 2 Hz force perturbation and control initiated 0.03 seconds late; —— (uncontrolled), ▬▬ (controlled).

5 Concluding Remarks

This paper addressed the development of a physics-based control methodology appropriate for magnetostrictive actuators in moderate to high drive level regimes. At such drive levels, these materials exhibit significant hysteresis and nonlinear dynamics which must be incorporated in the model and control method to attain the full potential of the actuator (both experiments and numerical simulations have demonstrated that linear methods fail at such drive levels). For various structural applications, it is also necessary to control both transient and steady state dynamics.

To attain these objectives, a model based upon ferromagnetic mean field theory was used to characterize the actuator dynamics including the inherent hysteresis and nonlinearities. This provided a method of accurately quantifying multiple frequencies and transient dynamics. Optimal control theory was then employed to obtain an open loop control which incorporated the actuator hysteresis and nonlinearities. This nonlinear control was combined with a perturbation feedback control to attain a hybrid method which was highly robust and efficient to implement. Finally, the efficacy of the method was demonstrated through numerical examples.

We note that the method described here does not address the minimum time control problem nor does it actively enforce admissibility criteria. If time minimization is desired, the control problem can be reformulated with the final time and final adjoint values treated as components of the solution. For applications which require that the control $u(t)$ lie in an admissible region, the stationary conditions (19) must be replaced by some form of the Pontryagin minimum principle. Details concerning both cases can be found in [6, 27].

In its present form, the method is currently designed for linear structural models. While it was illustrated in the context of a PDE-based thin beam model, the flexibility for employing large discretization limits in Matlab (in excess of 144 basis functions) indicates that the method can be directly applied to certain linear plate and shell models. For larger problems in which the number of spatial variables or time steps prohibits global optimization over the full time interval, piecewise methods of the type described in [20, 21] can be employed to obtain suboptimal solutions over each time step. These piecewise states and controls can then be patched together to obtain a global solution over the full time interval. Finally, we note that the extension of this method to nonlinear structural models is also important due to the advantages of high output actuators in such regimes and is under current investigation.

Acknowledgements

The author would like to thank H.T. Banks and K. Ito, North Carolina State University, for input and suggestions regarding the control methods considered here. Sincere thanks are also extended to F.T. Calkins, M. Dapino, A.B. Flatau and D. Jiles, Iowa State University, for extensive discussions regarding the construction, modeling and dynamics of magnetostrictive materials.

References

[1] U.M. Ascher, R.M.M. Mattheij and R.D. Russell, *Numerical Solution of Boundary Value Problems for Ordinary Differential Equations*, SIAM Classics in Applied Mathematics, 1995.

[2] H.T. Banks, W. Fang, R.J. Silcox and R.C. Smith, "Approximation methods for control of acoustic/structure models with piezoceramic actuators," *Journal of Intelligent Material Systems and Structures*, 4(1), 1993, pp. 98-116.

[3] S. Bittanti, A. Locatelli and C. Maffezzoni, "Periodic optimization under small perturbations," in *Periodic Optimization*, Vol. II, A. Marzollo, ed., Udine, Springer-Verlag, New York, 1972, pp. 183-231.

[4] M.D. Bryant, B. Fernández, N. Wang, V.V. Murty, V. Vadlamani and T.S. West, "Active vibration control in structures using magnetostrictive Terfenol with feedback and/or neural network controllers" Proceedings of the Conference on Recent Advances in Adaptive and Sensory Materials and their Applications (Technomic Publishing), Blacksburg, VA, April 27-29, 1992, pp. 465-479.

[5] M.D. Bryant and N. Wang, "Audio range controllability of linear motion Terfenol actuators," *Journal of Intelligent Material Systems and Structures*, 5, 1994, pp. 431-436.

[6] A.E. Bryson and Y-C. Ho, *Applied Optimal Control*, John Wiley and Sons, New York, 1975.

[7] J.L. Butler, "Application manual for the design of ETREMA Terfenol-D magnetostrictive transducers," EDGE Technologies, Inc., Ames, IA, 1988.

[8] F.T. Calkins, M.J. Dapino and A.B. Flatau, "Effect of prestress on the dynamic performance of a Terfenol-D transducer," Proceedings of the SPIE, Smart Structures and Materials 1997: Smart Structures and Integrated Systems, San Diego, CA, March 1997, Vol. 3041, pp. 293-304.

[9] F.T. Calkins, R.C. Smith and A.B. Flatau, "An energy-based hysteresis model for magnetostrictive transducers," *IEEE Transactions on Magnetics*, submitted.

[10] F.T. Calkins, R.L. Zrostlik and A.B. Flatau, "Terfenol-D vibration control of a rotating shaft," Proc. of the 1994 ASME International Mechanical Engineering Congress and Exposition, Chicago IL; In *Adaptive Structures and Composite Materials Analysis and Applications* AD-Vol. 45, 1996, pp. 267-274.

[11] A.E. Clark, "Magnetostrictive rare earth-Fe_2 compounds," Chapter 7 in *Ferromagnetic Materials*, Volume 1, E.P. Wohlfarth, editor, North-Holland Publishing Company, Amsterdam, pp. 531-589, 1980.

[12] G. Da Prato, "Synthesis of optimal control for an infinite dimensional periodic problem," *SIAM Journal of Control and Optimization*, 25(3), 1987, pp. 706-714.

[13] D.M. Dozer, M.J. Gerver and J.R. Swenbeck, "Nonlinear modeling for control of Terfenol-D based actuators," Proceedings of the SPIE, Smart Structures and Materials 1997: San Diego, CA, March 1997.

[14] W.S. Galinaitis and R.C. Rogers, "Compensation for hysteresis using bivariate Preisach models," Proceedings of the SPIE, Smart Structures and Materials 1997: Mathematics and Control in Smart Structures, San Diego, CA, March 1997.

[15] P. Ge and M. Jouaneh, "Tracking control of a piezoceramic actuator," *IEEE Transactions on Control Systems Technology,* 4(3), 1996, pp. 209-216.

[16] D.L. Hall and A.B. Flatau, "Nonlinearities, harmonics and trends in dynamic applications of Terfenol-D," Proceedings of the SPIE Conference on Smart Structures and Intelligent Materials, Vol. 1917, Part 2, 1993, pp. 929-939.

[17] D.L Hall and A.B. Flatau, "Analog feedback control for magnetostrictive transducer linearization," *Journal of Sound and Vibration*, to appear.

[18] M.W. Hiller, M.D. Bryant and J. Umegaki, "Attenuation and transformation of vibration through active control of magnetostrictive Terfenol," *Journal of Sound and Vibration*, 134(3), 1989, pp. 507-519.

[19] F.P. Hodges and J.M. Sewell, "Control of Terfenol actuators" Proceedings of the Conference on Recent Advances in Adaptive and Sensory Materials and their Applications (Technomic Publishing), Blacksburg, VA, April 27-29, 1992, pp. 457-464.

[20] L.S. Hou, S.S. Ravindran and Y. Yan, "Numerical solution of optimal distributed control problems for incompressible flows," *International Journal of CFD*, 8, 1997, pp. 99-114.

[21] L.S. Hou and Y. Yan, "Dynamics and approximations of a velocity field tracking problem for incompressible flows with piecewise distributed controls," *SIAM Journal of Control and Optimization,* 1997, to appear.

[22] A.G. Jenner, R.D. Greenough, D. Allwood and A.J. Wilkinson, "Control of Terfenol-D under load," *Journal of Applied Physics*, 76(10), 1994, pp. 7160-7162.

[23] D.C. Jiles, *Introduction to Magnetism and Magnetic Materials*, Chapman and Hall, New York, 1991.

[24] D.C. Jiles and D.L. Atherton, "Theory of ferromagnetic hysteresis," *Journal of Magnetism and Magnetic Materials*, 61, 1986, pp. 48-60.

[25] D.C. Jiles, J.B. Thoelke and M.K. Devine, "Numerical determination of hysteresis parameters for the modeling of magnetic properties using the theory of ferromagnetic hysteresis," *IEEE Transactions on Magnetics*, 28(1), pp. 27-35, 1992.

[26] E.B. Lee and L. Markus, *Foundations of Optimal Control Theory*, John Wiley and Sons, New York, 1967.

[27] F.L. Lewis and V.L. Syrmos, *Optimal Control*, John Wiley and Sons, New York, 1995.

[28] M. Moffet, A. Clark, M. Wun-Fogle, J. Linberg, J. Teter and E. McLaughlin, "Characterization of Terfenol-D for magnetostrictive transducers," *Journal of the Acoustical Society of America*, 89(3), pp. 1448-1455, 1991.

[29] A.V. Krishna Murty, M. Anjanappa and Y.-F. Wu, "The use of magnetostrictive particle actuators for vibration attenuation of flexible beams," *Journal of Sound and Vibration*, 206(2), pp. 133-149, 1997.

[30] E.R. Pinch, *Optimal Control and the Calculus of Variations*, Oxford University Press, Oxford, 1993.

[31] J. Pratt and A.B. Flatau, "Development and analysis of a self-sensing magnetostrictive actuator design," *Journal of Intelligent Material Systems and Structures*, 6(5), 1995, pp. 639-648.

[32] J.R. Pratt and A.H. Nayfey, "Boring-bar chatter control using a two-axes active vibration absorber scheme," Proceedings of Noise-Con 97, The Pennsylvania State University, University Park, PA, June 15-17, 1997, pp. 313-324.

[33] M.J. Sablik and D.C. Jiles, "Coupled magnetoelastic theory of magnetic and magnetostrictive hysteresis," *IEEE Transactions on Magnetics*, 29(3), pp. 2113-2123, 1993.

[34] R.C. Smith, "Modeling techniques for magnetostrictive actuators," CRSC Technical Report CRSC-TR97-6; Proceedings of the SPIE, Smart Structures and Materials 1997: Smart Structures and Integrated Systems, San Diego, CA, March 1997, Vol. 3041, pp. 243-253.

[35] R.C. Smith, "Well-posedness issues concerning a magnetostrictive actuator model," Proceedings of the Conference on Control and Partial Differential Equations, CIRM, Marseille-Luminy, France, June 1997, to appear.

[36] G. Tao and P.V. Kokotović, *Adaptive Control of Systems with Actuator and Sensor Nonlinearities*, John Wiley and Sons, New York, 1996.

[37] E. du Trémolet de Lacheisserie, *Magnetostriction: Theory and Applications of Magnetoelasticity*, CRS Press, Ann Arbor, 1993.

[38] W. Wang and I. Busch-Vishniac, "A high performance micropositioner based on magnetostriction principles," *Review of Scientific Instruments*, 63(1), 1992, pp. 249-254.